Iranica Journal of Energy & Environment 5 (4): 419-435, 2014
ISSN 2079-2115
IJEE an Official Peer Reviewed Journal of Babol Noshirvani University of Technology
DOI: 10.5829/idosi.ijee.2014.05.04.10

BUT

3E Analysis and GA-Based Multi Objective Optimization of an Ejector-Flash Tank-Absorption Refrigeration System Fuelled by Solar Energy

Fateme Ahmadi Boyaghchi and Reihaneh Taheri

Department of Mechanical Engineering, Faculty of Engineering,
Alzahra University, Deh Vanak, Tehran, Iran

Received: September 1, 2014; Accepted in Revised form: October 15, 2014

Abstract: This paper proposes and investigates an improved ejector-absorption refrigeration system for providing the cooling load of an office building. Performance hourly modeling of the system is performed based on modeling the hourly required cooling load and hourly solar insolation rate on July 21 with maximum solar insolation. The results indicate that during the given day thermodynamic coefficient of performance (COP_{th}) and exergetic coefficient of performance (COP_{exe}) increase 150 and 300%, respectively. While, the product cost per exergy unit of the whole system (c_{Ptot}) decreases 90%. The results of thermodynamic and thermoeconomic analysis determine effective design parameters on COP_{th}, COP_{exe} and c_{Ptot}. Also, single and multiple objectives optimizations are applied to maximize COPs and minimize c_{Ptot}. According to the results, the single objective optimization for maximizing COPs increases COPs by about 1.1% and decreases c_{Ptot} by about 7.4%. Moreover, single objective optimization for minimizing c_{Ptot} results in 2.2 and 11.5% decrease in COPs and c_{Ptot}, respectively. Finally, multiple objectives optimization for maximizing COPs and minimizing c_{Ptot} simultaneously causes about 1.9% decline in COPs while c_{Ptot} decreases 10.9%.

Key words: Absorption · Ammonia-water · Ejector · Exergoeconomic analysis · Hourly modeling · Genetic algorithm

INTRODUCTION

As the energy crises turns out to be more and more noteworthy, the use of renewable energy resources becomes more inevitable. Also, the available solutions for the global warming dilemma are either to optimize the energy consumption of devices or focus on renewable energy resources such as solar energy. In the particular scope of cooling systems, recent researches are focused on solar absorption refrigeration systems. Solar cooling is an attractive idea because cooling demand and availability of solar radiation are at the same time. Although the investment cost of absorption refrigeration systems is high, they are preferred to other cooling systems because their working fluids are not harmful to the environment [1]. Extensive research is carried out to increase efficiency of absorption refrigeration systems and decrease their costs simultaneously by means of improving system design such as using an ejector or improving design conditions through thermoeconomic analysis.

Several papers have published in field of solar absorption refrigeration systems. Alvares and Trepp [2] studied an ammonia-water absorption refrigeration system coupled with a compound parabolic collector. They optimized COP_{th} and COP_{exe} up to about 60% by examining different types of absorption refrigeration systems. The application of a solar single effect absorption refrigeration system for Antalya, Turkey was investigated by Atmaca and Yigit [3]. They analyzed the effect of temperature of hot water inlet to generator on COP and heat exchanger areas. Hourly analysis of a solar absorption refrigeration system was carried out by Ozgoren *et al*. [4] to study changes for COP and heat transfer of components during

Corresponding Author: Fateme Ahmadi Boyaghchi, Department of Mechanical Engineering, Faculty of Engineering, Alzahra University, Deh Vanak, Tehran, Iran.
Tel: +9821-88044040-2140, Fax: +9821-88617537.

Please cite this article as: Fateme Ahmadi Boyaghchi and Reihaneh Taheri, 2014. 3E Analysis and GA-Based Multi Objective Optimization of an Ejector-Flash Tank-Absorption Refrigeration System Fuelled by Solar Energy. Iranica Journal of Energy and Environment, 5 (4): 419-435.

the day. However hourly cost discussion is not done by these researchers. Hamed *et al*. [5] considered a dynamic theoretical study and optimization of a solar absorption refrigeration system to minimize the time required to reach a certain operation temperature in the refrigerated space while entropy generation is minimized and refrigeration rate is maximized.

In field of absorption refrigeration systems some researchers focused on developing absorption refrigeration system by adding ejector to increase COP of these systems. Sun *et al*. [6] in a new design used an ejector between the generator and condenser in a single effect water-lithium bromide absorption refrigeration system. They demonstrated 20-40% increase in COP after adding the ejector. This amount is announced about 60% by Aphornratana and Eames [7] due to experimental studying of adding ejector to absorption refrigeration systems. Hong *et al*. [8] presented an innovative design for a water- lithium bromide ejector-absorption refrigeration system. They proved that the ejector-absorption system leads to 10-30% higher COP in comparison to a single effect absorption system. On the other hand, researchers rarely discussed about using an ejector in solar absorption refrigeration systems. Sözen and Özalp [9] optimized a solar ammonia-water ejector-absorption refrigeration system in order to maximize COP and minimize the amount of auxiliary heat. They also investigated the possibility of using these kinds of systems for geographical characteristics of Turkey. Sirwan *et al*. [10, 11] studied the effect of adding a flash tank to a solar ammonia-water ejector-absorption refrigeration system on thermodynamic and exergetic COPs. As it is obvious adding flash tank causes improvement in the quality of refrigerant entering to the evaporator.

Thermoeconomic is a useful analyzing tool to examine a system economically beside thermodynamic aspects. In field of absorption refrigeration systems, cost optimization by means of thermoeconomic analysis is an interesting subject for most of recent studies. Misra *et al*. [12] applied thermoeconomic theory to a single effect water-lithium bromide absorption refrigeration system to minimize overall operation and amortization expenses through optimization. The results show 5% decrease in product cost per exergy unit and 10% increase in COP. Optimizing a water-lithium bromide single effect absorption refrigeration system has done by Rubio-Maya [13] to minimize the annual operating cost. Consequently, by decreasing annual operating cost the rate of exergy destruction is doubled. Garousi Farshi *et al*. [14] compared a double effect absorption refrigeration system with single effect ejector-absorption refrigeration in terms of thermoeconomic. By studying investment cost and product cost of flow rates in both systems they show the superiority of the single effect ejector-absorption refrigeration system.

In this study, the performance of a solar ammonia-water ejector-absorption refrigeration system for cooling of an office building located in Tehran is studied. The system is modeled hourly by computer codes according to different cooling loads and insolation rates during the day. The study is conducted on 21st of June which has the maximum insolation rate in the year. Thermodynamic and thermoeconomic analysis is applied to the system to recognize effective design parameters on thermodynamic COP, exergetic COP and product cost per exergy unit of the whole system (c_{Ptot}). Finally, by means of Genetic Algorithm, single and multiobjective optimizations are carried out to maximize COPs and minimize c_{Ptot}. The merit of this study is the thermodynamic and thermoeconomic hourly modeling of the solar absorption cooling system (depending on solar insolation and cooling load changes) that is a new approach compared to recent similar studies done by other researchers [10, 14].

Modeling: The schematic diagram of an ejector-absorption refrigeration system coupled with a solar collector is illustrated in Figure 1. In this cycle the evaporator is preparing a chilled water stream that is covering cooling load of an office building ($\dot{Q}_{eva}$) through several fan coils. The cycle contains ammonia refrigerant which enters to the evaporator (at point 1) and evaporates at exit. The refrigerant gets mixed with water in the absorber and a concentrated solution of ammonia in form of saturated liquid leaves the absorber (point 4) to get compressed by means of a pump. After achieving heat from the rectifier and the solution heat exchanger it goes into the generator. In the generator the saturated vapor of ammonia is extracted (at point 8) and dilute solution returns to the solution heat exchanger (point 19) to complete the absorption cycle. The refrigerant becomes more purified by passing through the rectifier and the saturated vapor of ammonia enters to the ejector as the primary fluid (point 10). After mixing with the secondary fluid that comes from the mix chamber, the outlet stream goes into the condenser to lose heat and become saturated liquid at the exit. In the flash tank, liquid and vapor phases are separated in saturated state to make a desirable refrigerant. On the other hand, the hot water supplied by an evacuated tube collector (at point 27) enters to the heat storage tank to warm the existing water

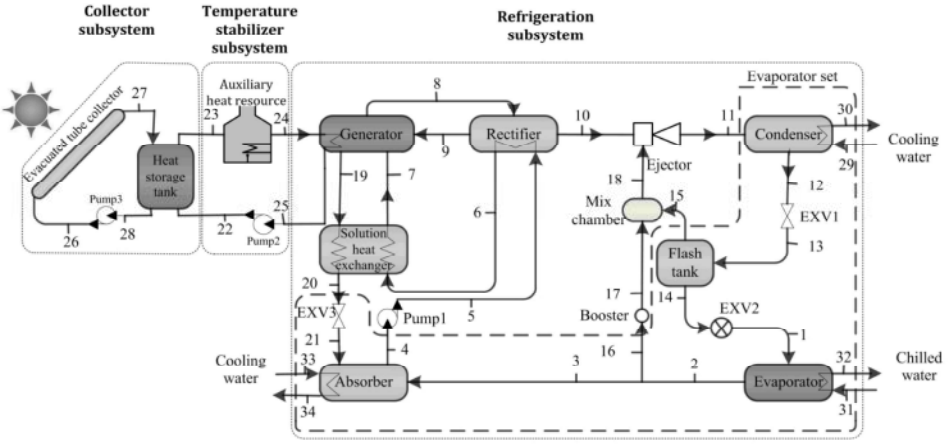

Fig. 1: Schematic diagram of a solar ejector-absorption refrigeration system

in the tank. The hot water at the exit of the heat storage tank (point 23) gains more heat from auxiliary heat resource if it is needed and inlet to the generator to supply its required heat ($\dot{Q}_{gen}$). Computer modeling in EES software [15] was carried out while considering the following assumptions for the system:

- The process in each component is considered to be steady state and steady flow process.
- Cooling processes in the absorber and condenser is done by two closed cooling water streams.
- The ammonia in the evaporator, condenser, ejector and flash tank has constant concentration (x_c).
- The working fluid in the collector and heat storage tank is compressed liquid water.
- The fluid leaves each component at the component temperature.

Thermodynamic Modeling

Energy Analysis: Considering each component as a control volume, mass and energy conservation equations are considered. Additionally mass balance for ammonia is considered separately by inserting concentration as a coefficient of mass in equation (2) [16].

$$\sum_{in} \dot{m}_i = \sum_{out} \dot{m}_o \tag{1}$$

$$\sum_{in} \dot{m}_i x_i = \sum_{out} \dot{m}_o x_o \tag{2}$$

$$\dot{Q} - \dot{W} = \sum_{out} \dot{m}_o h_o - \sum_{in} \dot{m}_i h_i \tag{3}$$

Where, $\dot{m}$ is mass flow rate (kg s^{-1}), x is ammonia-water concentration (kg kg^{-1}), $\dot{Q}$ is heat transfer rate (kW), h is power (kW) and h is specific enthalpy (kJ s^{-1}). The subscripts in and out refer to inlet and outlet flow stream. The inlet primary fluid to the ejector suctions the secondary fluid comes from the mix chamber into the ejector. Entrainment ratio which is the ratio of secondary mass fluid rate to primary mass fluid rate (ù) is a function of thermodynamic and physical characteristics of the ejector. In the present modeling the effect of the ejector performance on the entrainment ratio is considered by related relations extracted from Sun *et al*. study [6]. The inlet primary fluid passes sequentially through four different sections which are named nozzle section, mixing section, constant area section and diffuser section. At the beginning, the primary fluid expands irreversibly through the nozzle section and combines with the secondary fluid in the mixing section at constant pressure. By considering that a transverse shock happens at the constant area section which increases static pressure, the geometry of the ejector is determined. In continue the subsonic mixed flow is compressed further until its velocity reaches zero at the exit plane of the diffuser [6].

The auxiliary heat is supplied by a boiler which uses natural gas as fuel. The rate of produced heat by boiler is calculated by considering the lower heating value (LHV) of natural gas as below [17]:

$$\dot{Q}_{aux} = \eta_{aux} \dot{m}_{NG} LHV_{NG} \tag{4}$$

Where, $\dot{Q}_{aux}$ heat transfer rate of auxiliary heater (kW), $\dot{m}_{NG}$ mass flow rate of natural gas (kg s^{-1}), η_{aux} is efficiency of auxiliary heater and LHV_{NG} is the lower heating valve of natural gas (kJ). The amount of $\dot{Q}_{aux}$ is determined by the difference between the temperature of required hot water for the generator and the temperature of outlet water from the heat storage tank.

By considering the heat storage tank as an intermediate between the collector and the generator, the temperature of heat storage tank is calculated as below [1, 18, 19]: (T_{am} is ambient temperature which is considered as 25°C.)

$$T_{hst,t+1} = T_{hst,t} + \frac{\Delta t}{(Mc_p)_{hst}}[\dot{Q}_{coll} - \dot{Q}_{load} - (UA)_{hst}(T_{hst,t} - T_{am})] \quad (5)$$

$$\dot{Q}_{coll} = \dot{m}_C c_{p,w}(T_{27} - T_{28}) \quad (6)$$

$$\dot{Q}_{load} = \dot{m}_L c_{p,w}(T_{23} - T_{22}) \quad (7)$$

$$\dot{Q}_{hstl} = (UA)_{hst}(T_{hst} - T_{am}) \quad (8)$$

Where, T_{hst} is temperature of heat storage tank (K), $(Mc_p)_{hst}$ is the heat capacity of heat storage tank (kJ K^{-1}), Δt is time interval (K), $c_{p,w}$ is the specific capacity of water (kJ kg^{-1} K^{-1}) and $(UA)_{hst}$ is the overall heat transfer coefficient of heat storage tank (kW K^{-1}). For the evacuated tube collector, $\dot{Q}_{use}$ is considered as useful heat rate gained by water from solar insolation through collector [18].

$$\dot{Q}_{use} = \eta_{etc} A_a G_t \quad (9)$$

Where, η_{etc} is the efficiency of evacuated tube collector. A_a is the apparture area of collector (m^2) and G_t is the solar insolation rate (W s^{-1}) on the collector tilted surface that is described more in section ý2.3.1. An evacuated tube collector is suggested for an ammonia-water absorption refrigeration system by water cooling [1]. The collector efficiency η_{etc} of the used evacuated tube collector is calculated from the below equation [20]:

$$\eta_{etc} = \eta_0 - \frac{a_1(T_m - T_{air})}{G_t} - \frac{a_2(T_m - T_{air})^2}{G_t}, T_m = \frac{T_i + T_o}{2} \quad (10)$$

In this article the coefficient of the above equation are extracted from Apricus Company [21] for the evacuated tube collector model AP_30 with 2.82 m^2 aperture area.

$$\eta_0 = 0.656, a_1 = 1.4, a_2 = 0.007 \quad (11)$$

Exergy Analysis: Exergy is the maximum work that a system can do to reach to the thermodynamic dead state that is exactly equal to environment. Exergy is mainly consists of physical (ex^{PH}) and chemical (ex^{CH}) exergies [17].

$$ex = ex^{PH} + ex^{CH} \quad (12)$$

Physical exergy is defined as the maximum work is done by a system to transfer from the state with certain temperature and pressure to the reference environment state which is specified with subscript 0 in the below equation [17].

$$ex^{PH} = (h - h_0) - T_0(s - s_0) \quad (13)$$

Where, h is enthalpy (kJ kg^{-1}), T is temperature (K) and s is entropy (kJ kg^{-1} K^{-1}). The subscript 0 refer to reference state. In this article the liquid water at 25°C and 101.325 kPa is assumed to be as the reference environment. Chemical exergy is also defined as the maximum work is done by a system to transfer from reference environment to dead state. Chemical exergy of water in collector and temperature stabilizer subsystems is neglected and specific chemical exergy of ammonia-water solution is defined as [22]:

$$ex_{Sol}^{CH} = [\frac{\overline{ex}^0_{Ch,NH_3}}{M_{NH_3}}]x + [\frac{\overline{ex}^0_{Ch,H_2O}}{M_{H_2O}}](1 - x) \quad (14)$$

$\overline{ex}^0_{Ch,NH_3}$ and $\overline{ex}^0_{Ch,H_2O}$ are standard molar chemical exergy of ammonia and water which are extracted from references [17, 23] and M_{NH3} and M_{H2O} are molecular weight of ammonia and water, respectively.

In this study the Fuel-Product Method has been applied for exergy analysis. Fuel exergy rate($\dot{X}_F$) and product exergy rate ($\dot{X}_P$) are defined as required input and desired output respectively. Inefficiencies are measured by exergy loss rate ($\dot{X}_L$) and exergy destruction rate ($\dot{X}_D$). If the transfer process happens at constant temperature (T_k), the exergy loss is given by [17]:

$$\dot{X}_L = (1 - \frac{T_0}{T_k})\dot{Q}_k \, 0 \quad (15)$$

The exergy destruction, exergetic efficiency, exergy destruction ratios and exergy loss ratio are also calculated for the exergy analysis as following [17]:

$$\dot{X}_D = \dot{X}_F - \dot{X}_P - \dot{X}_L \quad (16)$$

$$\eta_{exe} = \frac{\dot{X}_P}{\dot{X}_F} = 1 - \frac{\dot{X}_D + \dot{X}_L}{\dot{X}_F} \quad (17)$$

Table 1: Definition of fuel exergy, product exergy and exergy loss of the solar ejector-absorption refrigeration system components

Name	$\dot{X}_F$	$\dot{X}_P$	$\dot{X}_L$
Evaporator set	$\dot{X}_{11}-\dot{X}_{15}-\dot{X}_{16}+\dot{X}_{20}-\dot{X}_4$	$\dot{X}_{32}-\dot{X}_{31}$	$\dot{X}_{30}-\dot{X}_{29}+\dot{X}_{34}-\dot{X}_{33}$
Solution heat exchanger	$\dot{X}_{19}-\dot{X}_{20}$	$\dot{X}_7-\dot{X}_6$	0
Generator	$\dot{X}_{24}-\dot{X}_{25}$	$\dot{X}_8-\dot{X}_7+\dot{X}_{19}-\dot{X}_9$	0
Rectifier	$\dot{X}_8-\dot{X}_{10}-\dot{X}_9$	$\dot{X}_6-\dot{X}_5$	0
Ejector	$\dot{X}_{10}+\dot{X}_{18}$	$\dot{X}_{11}$	0
Booster	$\dot{W}_{bst}$	$\dot{X}_{17}-\dot{X}_{16}$	0
Mix chamber	$\dot{X}_{15}+\dot{X}_{17}$	$\dot{X}_{18}$	0
Auxiliary heat resource	$\dot{X}_{NG}$	$\dot{X}_{24}-\dot{X}_{23}$	0
Heat storage tank	$\dot{X}_{27}+\dot{X}_{22}$	$\dot{X}_{23}+\dot{X}_{28}$	$\dot{X}_{hstl}$
Evacuated tube collector	$\dot{X}_{sun}$	$\dot{X}_{27}-\dot{X}_{26}$	0
Pump	$\dot{W}_{pmp}$	$\dot{X}_o-\dot{X}_i$	0

$$y_D=\frac{\dot{X}_D}{\dot{X}_{F,tot}},\ y_D^*=\frac{\dot{X}_D}{\dot{X}_{D,tot}} \tag{18}$$

$$y_L=\frac{\dot{X}_L}{\dot{X}_{F,tot}} \tag{19}$$

A proper 'Fuel Product Loss' (FPL) definition for each component of the system is necessary for an efficient exergy analysis to describe the actual nature of physical flows. In the refrigeration subsystem determining fuel and product roles is easy for the evaporator, solution heat exchanger, generator, rectifier, mix chamber and pumps where exergy of the product exergy is increased. On the other hand, for the absorber, condenser, flash tank and expansion valves special considerations are applied because of complicity of product defining. By considering Bejan *et al*. [17] methodology a single virtual component is considered as a representative of these components and is shown as evaporator set. Appling mentioned assumptions and related formulas presented in references [17, 22, 24], FPL definition of components are represented in Table 1.

The exergy rate of heat supplied by auxiliary heat resource is calculated as below [17]: ($\overline{\text{ex}}^{0}_{\text{CH,NG}}$ is standard molar chemical exergy of natural gas which considered 824348 kJ/kmol extracted from Bejan *et al*. [17].

$$\dot{X}_{NG}=\dot{m}_{NG}R_{NG}T_0\ln(\frac{P_{NG}}{P_0})+\dot{m}_{NG}\frac{\overline{ex}^{0}_{CH,NG}}{M_{NG}} \tag{20}$$

The exergy loss of heat storage tank is calculated by equation (15) and the input solar exergy is considered as following while T_{sun} is assumed to be 6000 K [25]:

$$\dot{X}_{sun}=G_tA_a(1+\frac{1}{3}(\frac{T_0}{T_{sun}})^4-\frac{4}{3}(\frac{T_0}{T_{sun}})) \tag{21}$$

The Thermodynamic coefficient of performance (COP_{th}) is considered for the system as the ratio of the energy extracted from chilled water through the evaporator to the total energy supplied to the system [12].

$$COP_{th}=\frac{\dot{Q}_{eva}}{A_aG_t+\dot{m}_{NG}LHV_{NG}+\sum_{pmp1,2,3,bst}\dot{W}} \tag{22}$$

The exergetic coefficient of performance (COP_{exe}) is defined same for the system as:

$$COP_{exe}=\frac{\dot{X}_{32}-\dot{X}_{31}}{\dot{X}_{sun}+\dot{X}_{NG}+\sum_{pmp1,2,3,bst}\dot{W}} \tag{23}$$

Thermoeconomic Modeling: Cost balance for each component indicates that the sum of cost rates associated with all exiting streams equals the sum of cost rates of all entering streams plus capital investment and operating and maintenance (O&M) costs rates. Considering heat is received and work is produced by a component the cost balance equation would be [17]:

$$\sum_{out}c_o\dot{X}_o+c_w\dot{X}_w=c_q\dot{X}_q+\sum_{in}c_i\dot{X}_i+\dot{Z}$$
$$\dot{Z}=\frac{Z^{CI}+Z^{OM}}{ta} \tag{24}$$

By considering the above equation for all components and some auxiliary relations [17, 22, 26, 27] summarized in Table 2 cost per exergy unit of all streams can be found.

The cost rate of exergy loss is calculated by considering that the rate of product exergy is constant [17].

Table 2: The cost balances and auxiliary relations of the solar ejector-absoption refrigeration system

Component	Cost balance	Auxiliary relation
Evaporator set	$\dot{C}_{30}+\dot{C}_{32}+\dot{C}_{34}+\dot{C}_{15}+\dot{C}_{16}+\dot{C}_4=$ $\dot{C}_{29}+\dot{C}_{31}+\dot{C}_{33}+\dot{C}_{11}+\dot{C}_{20}+\dot{Z}_{eva}+\dot{Z}_{abs}+\dot{Z}_{con}+\dot{Z}_{flt}+\sum_{1,2,3}\dot{Z}_{exv}$	$c_{30}=c_{33}$ $c_{16}=c_2, c_3=c_2$
	$\dot{C}_2+\dot{C}_{32}=\dot{C}_1+\dot{C}_{31}+\dot{Z}_{eva}$	$c_2=c_1$
	$\dot{C}_4+\dot{C}_{34}=\dot{C}_3+\dot{C}_{21}+\dot{C}_{33}+\dot{Z}_{abs}$	$\frac{\dot{C}_4}{\dot{X}_4}=\frac{\dot{C}_3+\dot{C}_{21}}{\dot{X}_3+\dot{X}_{21}}$
	$\dot{C}_{30}+\dot{C}_{12}=\dot{C}_{11}+\dot{C}_{29}+\dot{Z}_{con}$	$c_{11}=c_{12}$
	$\dot{C}_{15}+\dot{C}_{14}=\dot{C}_{13}+\dot{Z}_{flt}$	
	$\dot{C}_o=\dot{C}_i+\dot{Z}_{exv}$	
Solution heat exchanger	$\dot{C}_{20}+\dot{C}_7=\dot{C}_{19}+\dot{C}_6+\dot{Z}_{she}$	$c_{20}=c_{19}$
generator	$\dot{C}_{19}+\dot{C}_8+\dot{C}_{25}=\dot{C}_7+\dot{C}_9+\dot{C}_{24}+\dot{Z}_{gen}$	$\frac{\dot{C}_8-\dot{C}_7}{\dot{X}_8-\dot{X}_7}=\frac{\dot{C}_{19}-\dot{C}_7}{\dot{X}_{19}-\dot{X}_7}, c_{24}=c_{25}$
Rectifier	$\dot{C}_6+\dot{C}_{10}+\dot{C}_9=\dot{C}_8+\dot{C}_5+\dot{Z}_{rec}$	$\frac{\dot{C}_{10}-\dot{C}_8}{\dot{X}_{10}-\dot{X}_8}=\frac{\dot{C}_9-\dot{C}_8}{\dot{X}_9-\dot{X}_8}, c_6=c_5$
Ejector	$\dot{C}_{11}=\dot{C}_{10}+\dot{C}_{18}+\dot{Z}_{ejc}$	-
Booster	$\dot{C}_{17}=\dot{C}_{16}+\dot{C}_{w,bst}+\dot{Z}_{bst}$	$\dot{C}_{w,bst}=c_{elec}\dot{W}_{bst}$
Mix chamber	$\dot{C}_{18}=\dot{C}_{15}+\dot{C}_{17}+\dot{Z}_{mix}$	-
Auxiliary heat resource	$\dot{C}_{24}=\dot{C}_{23}+\dot{C}_{q,aux}+\dot{Z}_{aux}$	$\dot{C}_{q,aux}=c_{NG}\dot{X}_{aux}$
Heat storage tank	$\dot{C}_{23}+\dot{C}_{28}+\dot{C}_{hstl}=\dot{C}_{22}+\dot{C}_{27}+\dot{Z}_{hst}$	$c_{23}=c_{28}$ 0
Evacuated tube collector	$\dot{C}_{27}=\dot{C}_{26}+\dot{C}_{sun}+\dot{Z}_{etc}$	$\dot{C}_{sun}=0$
Pump	$\dot{C}_o=\dot{C}_i+\dot{C}_{w,pmp}+\dot{Z}_{pmp}$	$\dot{C}_{w,pmp}=c_{elec}\dot{W}_{pmp}$

$$\dot{C}_L=c_F\dot{X}_L \tag{25}$$

Considering the cost balance as the below equation [17] and considerations discussed in previous section fuel and product cost rates of all components can be developed.

$$\dot{C}_P=\dot{C}_F-\dot{C}_L+\dot{Z} \tag{26}$$

Thermoeconomic evaluation is done by means of five important thermoeconomic variables which are namely; cost per exergy unit of fuel (c_F), cost per exergy unit of product (c_P), cost rate of exergy destruction ($\dot{C}_D$), relative cost difference (r) and exergoeconomic factor (f) and calculated as below [17]:

$$c_F=\frac{\dot{C}_F}{\dot{X}_F} \tag{27}$$

$$c_P=\frac{\dot{C}_P}{\dot{X}_P} \tag{28}$$

$$\dot{C}_D=c_F\dot{X}_D, (\dot{X}_P=cte) \tag{29}$$

$$r=\frac{c_P-c_F}{c_F} \tag{30}$$

$$f=\frac{\dot{Z}}{\dot{Z}+c_F(\dot{X}_D+\dot{X}_L)} \tag{31}$$

The cost per exergy unit of product can be considered for the overall system as following:

$$c_{Ptot}=\frac{\dot{C}_{32}-\dot{C}_{31}}{\dot{X}_{32}-\dot{X}_{31}} \tag{32}$$

The procedure that is used to calculate the capital investment and O&M cost rate is explained in Appendix A.1.

Hourly Climate Data

Solar Insolation: Necessary equations for calculating the solar insolation on the collector tilted surface (G_t) are taken from Kalogirou [1]. G_t is calculated by the below equation through total insolation on horizontal surface (G), diffuse insolation on horizontal surface (G_D) and other parameters which are described as below:

$$\frac{G_t}{G} = (1-\frac{G_D}{G})R_B + \frac{G_D}{G}(\frac{1+\cos(\beta_c)}{2}) + \rho_G(\frac{1-\cos(\beta_c)}{2}) \quad (33)$$

$$R_B = \frac{\sin(L-\beta_c)\sin(\delta)+\cos(L-\beta_c)\cos(\delta)\cos(h)}{\sin(L)\sin(\delta)+\cos(L)\cos(\delta)\cos(h)} \quad (34)$$

Where, R_B is beam radiation tilt factor, β_c is incident angle of the collector (°), ρ_G is ground reflectance albedo, L is latitude (°), δ is declination (°) and h is hour angle (°). The data used in the calculation process are the amount of daily total insolation incident on a terrestrial horizontal surface (H) and daily average insolation clearness index ($\overline{K}_T$). These data are extracted from Atmospheric Science Data Center of NASA [28] for Tehran with geographical coordinates of 35.69 North latitude and 51.4 East longitude. Also daily diffuse insolation (H_D) and beam insolation on horizontal surface (G_B) can be calculated as below [1]:

$$\frac{H_D}{H} = 1.390 - 4.027\overline{K}_T + 5.531\overline{K}_T^2 - 3.108\overline{K}_T^3 \quad (35)$$

$$G_B = G - G_D \quad (36)$$

To extract the hourly values of total insolation from the daily values, the ratio of hourly total insolation to daily total insolation (r) is calculated as below [1]:

$$r = \frac{\pi}{24}[\alpha+\beta\cos(h)]\frac{\cos(h)-\cos(h_{ss})}{\sin(h_{ss})-(\frac{2\pi h_{ss}}{360})\cos(h_{ss})}$$
$$\alpha = 0.409+0.5016\sin(h_{ss}-60), \beta = 0.6609-0.4767\sin(h_{ss}-60) \quad (37)$$

Also by considering hour angle (h) and sunset hour angle (h_{ss}) in degrees, the ratio of hourly diffuse insolation to daily diffuse insolation (r_D) is calculated:

$$r_D = (\frac{\pi}{24})\frac{\cos(h)-\cos(h_{ss})}{\sin(h_{ss})-(\frac{2\pi h_{ss}}{360})\cos(h_{ss})} \quad (38)$$

Cooling Load: The Radiant time series method is applied to calculate the hourly cooling load of a specific office building in Tehran. The cooling load is defined as the rate at which the energy must be removed from a space to maintain the temperature and humidity at the design values. Different forms of heat gains which occur for the building at each hour in a day are calculated by the following equations [29]:

$$\dot{Q}_{window,rad} = [SHGC_{gB}A_{sl,g} + SHGC_f A_{sl,f}]G_B + [SHGC_{gD}A_g + SHGC_f A_f]G_D \quad (39)$$

Table 3: Radiative and convective fractions

Heat gain type	Radiative fraction (%)	Convective fraction (%)
Wall and window conduction	63	37
Roof conduction	84	16
People	70	30
Lighting	67	33
Equipment	20	80
Transmitted solar heat gain	100	0
Infiltration	0	100

$$\dot{Q}_{window,cond} = (U_f A_f + U_g A_g)(T_{out} - T_{in}) \quad (40)$$

$$\dot{Q}_{wall/roof,cond} = A_{wall/roof}\sum_{n=0}^{23} Y_{Pn}(T_{e,t-n\delta} - T_{rc}) \quad (41)$$

$$\dot{Q}_{\inf} = \frac{\dot{V}}{\upsilon_{out}}(T_{out} - T_{in}) \quad (42)$$

Where SHGC is solar heat gain coefficient. T_{out} and T_{in} are outlet and inlet temperature. The subscripts g, sl, f, B and D refer to glass element of window, sunlit area of window, frame element of window, beam radiation and diffused radiation, respectively. $\dot{Q}_{\inf}$ is infiltration heat rate (W), $\dot{V}$ is volumetric flow rate ($m^3 s^{-1}$) and υ_{out} is specific volume of outlet air ($m^3 kg^{-1}$). Y_{Pn} is defined as nth response factor and $T_{e,\ t\text{-}n\delta}$ is sol-air temperature at n hours ago which is calculated as [29]:

$$T_e = T_{out} + \frac{sa\times G}{h_{out}} - TRCT \quad (43)$$

Where, sa is solar absorptivity of surface, h_{out} is combined convection and radiation coefficient and TRCT is thermal radiation correction term (°). Heat gains from lights, equipment and humans are also considered for a common office building with 10 occupants who work from 9 AM to 5 PM. Each heat gain must be split into radiative and conductive portions which are considered as below [29]. Table 3 summarized radiative and convective factions.

Radiant time factor (r_n) is used to calculate the cooling load based on the current and past values of radiative heat gains [29].

$$\dot{Q}_{rad,cooling} = r_0\dot{Q}_t + r_1\dot{Q}_{t-\delta} + r_2\dot{Q}_{t-2\delta} + ... + r_{23}\dot{Q}_{t-23\delta} \quad (44)$$

Finally, the cooling load is determined by aggregating the cooling load due to the radiative portion with the convective portion of the heat gains. The building features and assumed parameters for cooling load calculation are explained in Appendix A.2.

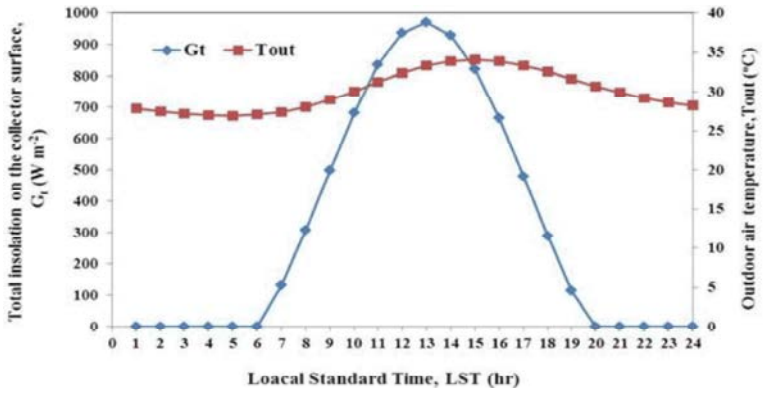

Fig. 2: Hourly variation of insolation on tilted collector surface and air temperature (The incidence angle of the collector is taken as 13°)

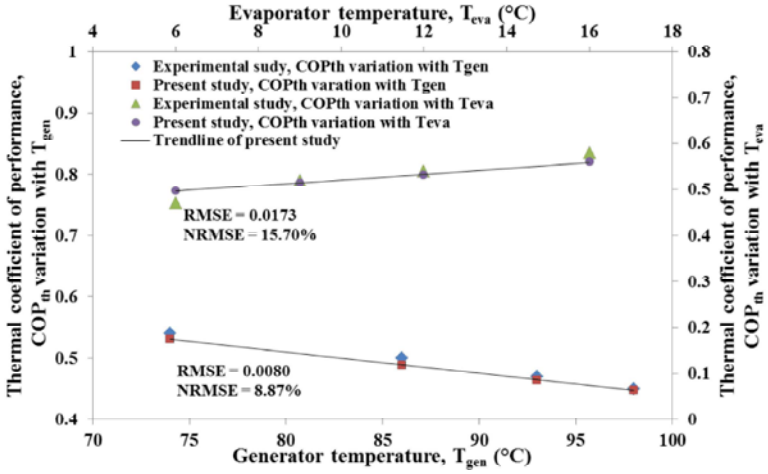

Fig. 3: Validation of the present study results against the experimental study values

As it is obvious, cooling load is strongly dependent to solar insolation and outdoor air temperature. The approximately same variation of hourly outdoor air temperature and solar insolation on tilted collector surface on 21st of Jun can be seen in Figure 2. Maximum value of outdoor air temperature is 34.11°C at 15 o'clock and the maximum value of the insolation on tilted collector surface is 960 W/m^2 at 13 o'clock.

Validation: For validation the results calculated by the present study model are compared with the experimental values extracted from Abdulateef *et al*. [30] work. For both cases the variation of the thermal COP with the generator temperature and the evaporator temperature are shown in Figure 3. The Root Mean Square Error (RMSE) and the Normalized RMSE (NRMSE) are used to measure the difference between present study results and the experimental values. According to the values of NRMSE shown on Figure 3 beside each diagram, the present study results are found to be in good agreement with experimental values with error no more than 16%. It means that the model is effective to analyze the performance of the solar ammonia-water ejector-absorption refrigeration system.

RESULTS AND DISCUSSION

In this article hourly modeling of an ejector-absorption refrigeration system used for cooling of an office building in Tehran is done through EES software [15]. Also Thermodynamic and thermoeconomic sensitivity analysis and optimization are carried out. Tables 4 and 5 represent the results of respectively exergy and thermoeconomic analysis of the system components for the climate data appeared at 13 o'clock on 21st of Jun and under the design conditions of the base case (T_{eva}=10°C, T_{abs}= T_{con}= 30 °C, T_{gen}= 85 °C, P_{gen}= 1800 kPa and x_c=0.9996).

Table 4: Exergy analysis results for the base case of the solar ejector-absorption refrigeration system

Name	$\dot{X}_F$ (kW)	$\dot{X}_P$ (kW)	$\dot{X}_D$ (kW)	$\dot{X}_L$ (kW)	yD(%)	yD*(%)	yL(%)	η_{exe}(%)
Evaporator set	0.87	0.06	0.74	0.07809	3.273	3.305	0.347	6.49
Solution heat exchanger	0.22	0.11	0.11	0	0.505	0.510	0	48.48
Generator	1.17	1.12	0.06	0	0.251	0.253	0	95.18
Rectifier	0.07	0.01	0.05	0	0.242	0.244	0	19.10
Ejector	1.21	1.09	0.12	0	0.519	0.524	0	90.32
Booster	0.01	0.01	0.00	0	0.000	0.001	0	99.01
Mix chamber	0.10	0.10	0.00	0	0.002	0.002	0	99.60
Auxiliary heat resource	2.07	0.32	1.75	0	7.776	7.851	0	15.38
Heat storage tank	5.79	4.30	1.41	0.08023	6.246	6.306	0.356	74.28
Evacuated tube collector	20.41	1.79	18.62	0	82.640	83.430	0	8.76
pumps	0.04	0.04	0.00	0	0.02	0.02	0	91.19

Table 5: Thermoeconomic results for the base case of the solar ejector-absorption refrigeration system

Name	c_F(\$/MJ)	c_P(\$/MJ)	$\dot{C}_D$(\$/Year)	$\dot{C}_L$(\$/Year)	$\dot{Z}$(\$/Year)	$\dot{Z}+\dot{C}_D+\dot{C}_L$(\$/Year)	f	r
Evaporator set	2.428	3.040	5158.08	546.05	651.17	6355.30	0.10	0.25
Solution heat exchanger	3.063	6.500	1004.26	0	56.07	1060.33	0.05	1.12
Generator	1.719	1.830	280.08	0	75.48	355.56	0.21	0.06
Rectifier	0.421	2.933	66.04	0	26.99	93.03	0.29	5.97
Ejector	2.066	2.287	695.23	0	0.00	695.23	0.00	0.11
Booster	0.012	2.247	0.00	0	72.35	72.35	1.00	187.19
Mix chamber	2.313	2.323	2.58	0	0.00	2.58	0.00	0.00
Auxiliary heat resource	0.004	0.470	21.55	0	396.29	417.84	0.95	109.07
Heat storage tank	2.206	3.006	8945.28	509.76	950.98	10406.02	0.09	0.36
Evacuated tube collector	0	0.425	0	0	2188.80	2188.80	1.00	infinity
pumps	0.036	4.444	0.13	0	116.35	64.11	1.00	123.06

The results show maximum exergy loss rate of 0.08 kW for the heat storage tank with y_L of 0.356%. The exergy destruction rate of the collector is 18.62 kW with y_D^* of 83.43% which is the maximum among all components. The high value of exergy destruction in the collector is because of irreversibility due to temperature difference. This phenomenon also leads to low exergy efficiency of 8.76%. After the collector, the auxiliary heat resource and heat storage tank have more exergy destruction than other components.

According to the thermoeconomic results shown in Table 5, the heat storage tank and evaporator have the highest value of $\dot{Z}+\dot{C}_D+\dot{C}_L$ and therefore the most important components from the thermoeconomic viewpoint. The low values of f for the heat storage tank and the evaporator set show that their costs are almost due to exergy destruction. By reducing heat loss in the heat storage tank, exergy destruction can be avoided. Also higher evaporator design temperature leads to less exergy destruction for the evaporator set. The most amount of capital investment and O&M costs rate of the whole system is allocated to the evacuated tube collector with about 48%. As the fuel cost per exergy unit of the collector is assumed to be zero, its relative cost difference is infinity. Comparing cost per exergy unit of product for different components shows that solution heat exchanger has the highest value while the collector has the lowest.

Thermodynamic and Thermoeconomic Hourly Analysis Results: Hourly analysis of a solar refrigeration system performance is important because cooling load and heat gained by the collector are affected by solar insolation rate changes during the day. By considering working hours from 9 AM to 5 PM on 21st of June and the base case design conditions, the hourly analysis results are illustrated in Figure 4-7. The hourly variation of heat transfer rates and the heat storage tank temperature are plotted in Figure 4. As it is predictable, the heat transfer rate gained by the collector ($\dot{Q}_{use}$) has the same trend as solar insolation. It increases 96% form 9 o'clock to the maximum value of 11.8 kW at 13 and then decreases.

The evaporator heat transfer rate ($\dot{Q}_{eva}$) increases 40% during the working hours and reach 4.25kW at 17. Although the solar insolation decreases after 12 o'clock, the cooling load is still increasing due to high value of outdoor air temperature. By increasing the demand cooling load in the evaporator the generator heat transfer supplies more energy. Therefore the generator heat

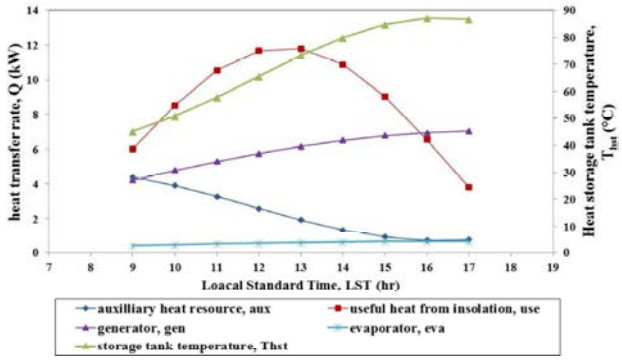

Fig. 4: Variation of heat transfer rates in the collector, evaporator, generator, auxiliary heat resource and heat storage tank temperature during the day

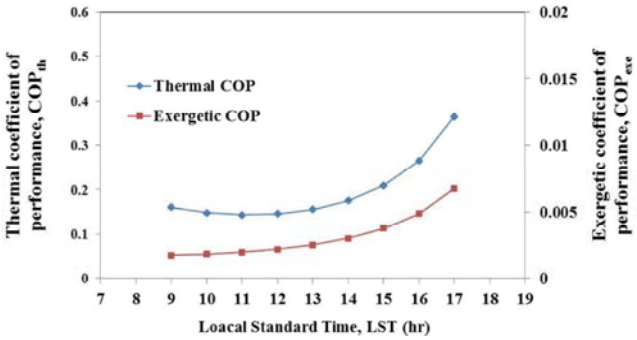

Fig. 5: Variation of thermal and exergetic coefficient of performance during the day

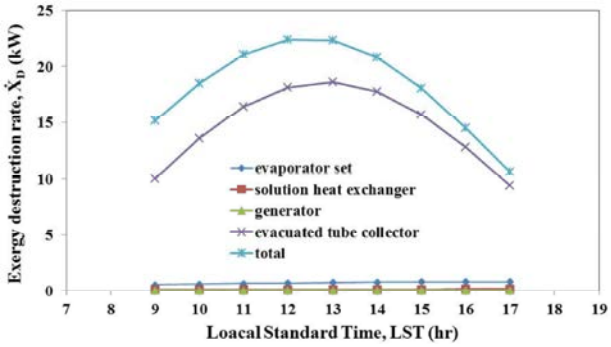

Fig. 6: Variation of exergy destruction rate of components and whole system during the day

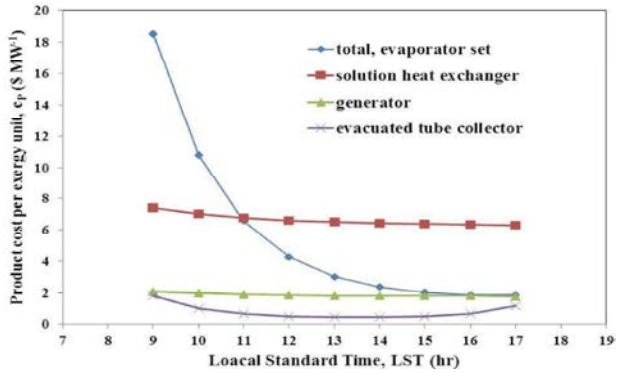

Fig. 7: Variation of product cost per exergy unit of components and whole system during the day

transfer rate ($\dot{Q}_{gen}$) follows the evaporator heat transfer rate changes by 67% increase. By way of contrast, the auxiliary heat transfer rate ($\dot{Q}_{aux}$) decreases about 83% during the working hours. Since at early hours of the day the temperature of heat storage tank is much lower than the temperature of hot water required for generator, auxiliary heat resource supplies more amount of the generator required heat than the heat storage tank. So the most amount of $\dot{Q}_{use}$ is consumed to increase the temperature of heat storage tank (T_{hst}) which causes considerable decrease in amount of $\dot{Q}_{aux}$ by time. At the end of the day $\dot{Q}_{aux}$ increases again to cover the heat storage tank temperature decline due to solar insolation decrease.

According to Figure 5, the amount of COP_{th} increases about 150% during the working hours. It is approximately constant from 9 o'clock to 13 while increases rapidly from 13 to 17 due to simultaneously increase of the evaporator heat transfer rate and decrease of the collector and auxiliary heat transfer rate. COP_{exe} has same trend while increases more (about 300%) because it is highly affected by solar insolation exergy. In Figure 6 Total exergy destruction rate increases about 47% to reach 22.39 kW at 12 o'clock and decreases to 10.65 kW at 17. The collector exergy destruction rate has exactly the same trend while the exergy destruction rate of the evaporator set, generator and solution heat exchanger increases about 50% to 70% during the day due to ascending trend of the evaporator and generator heat transfer rates.

According to Figure 7, the product cost per exergy unit decreases about 90% for the whole system which means by increasing the cooling load the product cost per exergy unit of whole system decreases. Because of solar insolation exergy changes, the collector product cost perexergy unit decreases about 76% from 9 O'clock to 13 while increases to reach 1.149 $/MW at 17. It means for more values of solar insolation the collector product costs less.

The amount of product cost per exergy unit of solution heat exchanger and generator decreases about 14% during the day. This means that their product costs are more affected by cooling load changes than solar insolation changes.

Thermodynamic and Thermoeconomic Sensitivity Analysis Results: In Figure 8-13, the variation of the generator and auxiliary heat resource heat transfer rates, COPs, cost per exergy unit and exergy destruction rate are studied under seven different design conditions. The results are considered for the climate data appeared at 13 o'clock on 21st of Jun. According to Figure 8, by increasing the generator temperature (T_{gen}) from 85 to 95 °C, heat transfer rate of the generator ($\dot{Q}_{gen}$) increases about 6% because the difference between temperature of inlet and outlet streams rises. The evaporator temperature increment (T_{eva}) from 8 to 12 °C, declines $\dot{Q}_{gen}$ by 44%. High values of the evaporator temperature lead to less amount of supply heat. The growth of generator pressure (P_{gen}) from 1750 to 1850 kPa, causes only 3% decrease. Also by increasing the ammonia-water solution concentration (x_C) from 0.9996 to 0.9998, $\dot{Q}_{gen}$ decreases about 14%.

Figure 9 reveals 38% growth in $\dot{Q}_{aux}$ by increasing T_{gen}. Also T_{eva}, P_{gen} and x_c growth leads to respectively 4%, 2% and 8% decrease in $\dot{Q}_{aux}$. The generator heat transfer change has a direct influence on the auxiliary heat transfer so $\dot{Q}_{aux}$ has the same trend as $\dot{Q}_{gen}$.

The Effect of Variable Design Conditions on COPs: According to Figure 10, it is seen that the generator temperature increase leads to 3.1% decline in COP_{th} due to the growth that happens in $\dot{Q}_{aux}$ while the cooling load is constant. The design temperature of the generator determines the efficiency of the whole system and for higher values of that, thermal efficiency steps down due to more required input energy. Increasing T_{eva}, P_{gen} and x_c causes respectively 0.4%, 0.1% and 0.9% increase in COP_{th} that is related to reduction of $\dot{Q}_{aux}$. In Figure 11 the obtained results for COP_{exe} are approximately as same as COP_{th} but its values are comparably low because of large amount of solar insolation exergy. The input solar exergy is independent to the generator temperature changes while the input boiler exergy increases due to more required energy. More required energy is supplied by increasing the mass flow rate of natural gas.

The Effect of Variable Design Conditions on C_{ptot} and Exergy Destruction: The variation of product cost per exergy unit of whole system is plotted in Figure 12. By increasing the generator temperature c_{Ptot} decreases 6.3% and T_{eva}, P_{gen} and x_c growth leads to respectively 3.3, 1.4 and 5.8% decrease. Although there are some complicated reasons for c_{Ptot} behaviors, it can be seen that for low generator temperatures COPs and $c_{P,tot}$ are simultaneously high. Moreover total exergy destruction rate variation ($\dot{X}_{Dtot}$) under different design conditions is illustrated in Figure 13. As it is predictable, its trend is exactly in

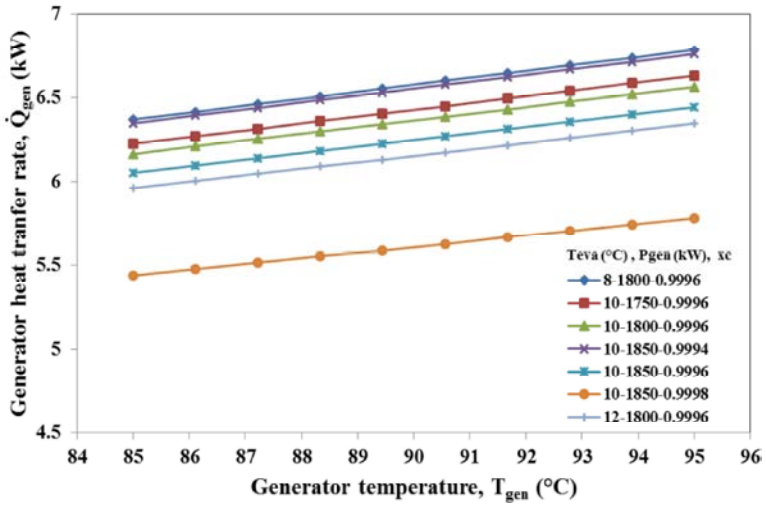

Fig. 8: Variation of the generator heat transfer rate with generator temperature under different design conditions

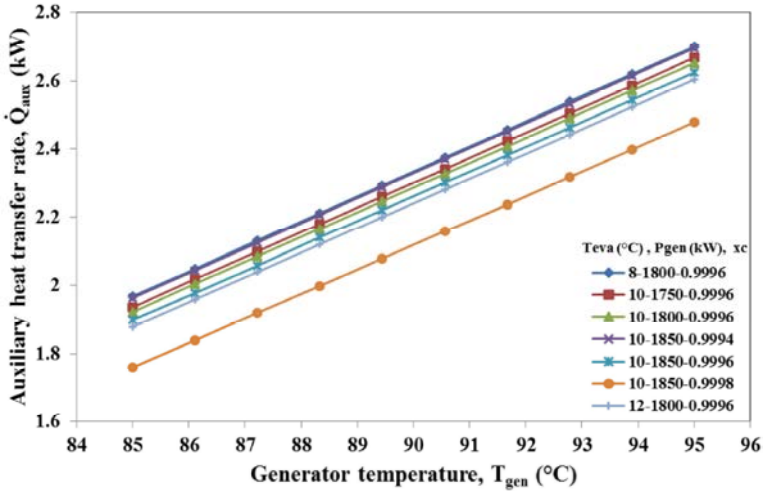

Fig. 9: Variation of the auxiliary heat transfer rate with generator temperature under different design conditions

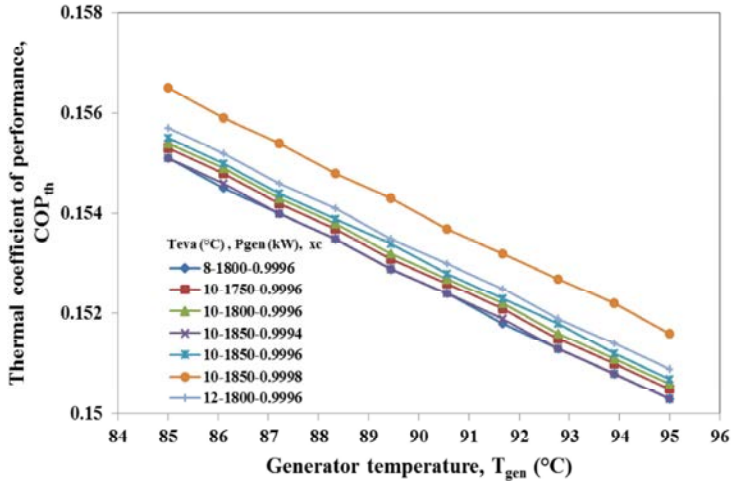

Fig. 10: Variation of thermal coefficient of performance with generator temperature under different design conditions

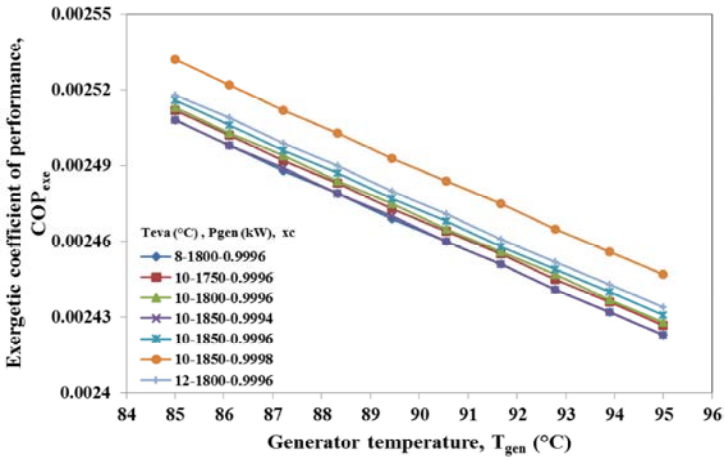

Fig. 11: Variation of exergetic coefficient of performance with generator temperature under different design conditions

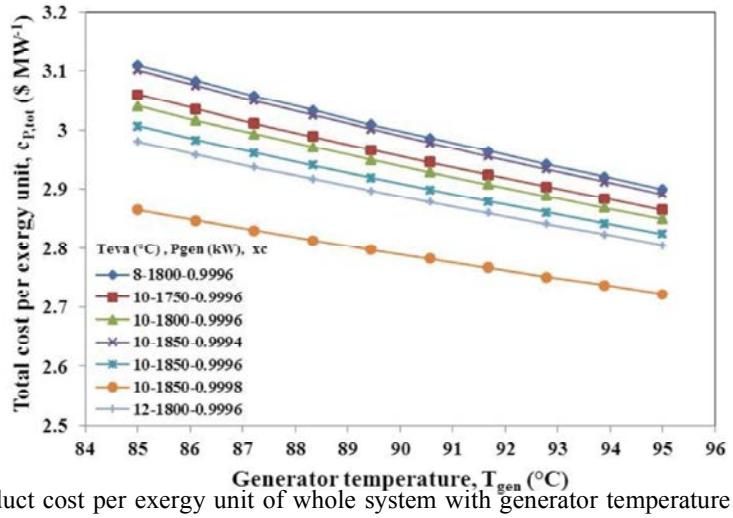

Fig. 12: Variation of product cost per exergy unit of whole system with generator temperature under different design conditions

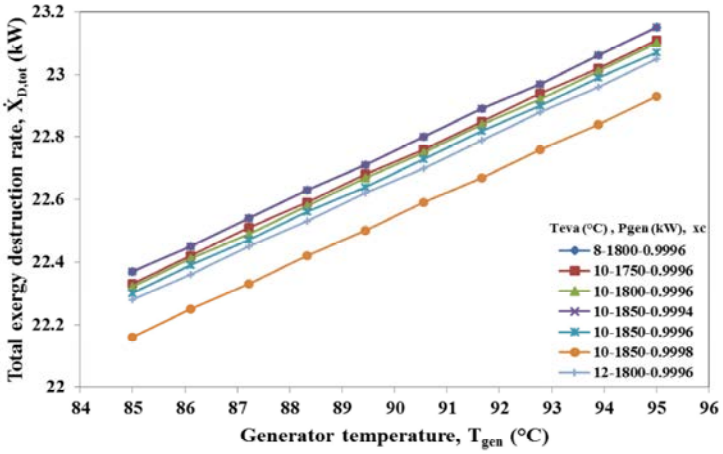

Fig. 13: Variation of exergy destruction rate of the whole system with generator temperature under different design conditions

Table 6: The Genetic Algorithm assumptions

Name	Amount
Number of individuals	32
Number of generations	128
Maximum rate of mutation	0.2625

Table 7: The range of decision variables

Variable name	Symbol	Range
Evaporator temperature	Teva	8 - 12 °C
Generator temperature	Tgen	85 - 95 °C
Generator pressure	Pgen	1750 - 1850 kpa
Ammonia concentration	xc	0.9994 - 0.9998

Table 8: The values of objective functions for various cases

		Single objective optimized state						Multiple objective optimized state	
Decision variable	Base case	Maximum COP_{th}	Difference (%)	Maximum COP_{exe}	Difference (%)	Minimum c_{Ptot}	Difference (%)	Maximum F	Difference (%)
COP_{th}	0.1554	0.1570	1.03	0.1570	1.03	0.1522	-2.06	0.1525	-1.87
COP_{exe}	0.00251	0.00254	1.11	0.00254	1.11	0.00245	-2.27	0.00246	-2.03
$c_{Peva\ set}$ ($ MJ^{-1})	3.0400	2.8160	-7.37	2.8160	-7.37	2.6920	-11.45	2.7060	-10.99

contrast with COPs trend in Figure 10 and 11. By increasing T_{gen} the amount of $\dot{X}_{Dtot}$ increases about 3.5% while T_{eva}, P_{gen} and x_c growth causes respectively 0.4, 0.2 and 0.9% reduction. Although the most fraction of input exergy to the system is related to the solar insolation exergy that is independent to the generator temperature changes, the input exergy form the auxiliary heat resource side has small effect on the total exergy destruction. It means by increasing the generator temperature the input auxiliary exergy increases which causes more irreversibility for whole system.

Optimization: COPs and $c_{P,tot}$ represent performance of the system and product cost respectively. Optimization of them will result to higher performance with a lower cost which is essential for the system. This is a multiobjective optimization problem that could be simplified into a single objective optimization through weighted sum method. This method introduces a weighted sum of all the objectives as a combined objective function [31]:

$$\begin{aligned} &Max(F(T_{gen},T_{eva},P_{gen},x_c)=w_1COP_{th}+w_2COP_{exe}+w_3(1-c_{P,tot}))\\ &0\le w_1\le 1,\\ &0\le w_2\le 1,\\ &0\le w_3\le 1,\\ &w_1+w_2+w_3=1 \end{aligned} \quad (45)$$

Where w_1, w_2 and w_3 are weighting factors for thermodynamic, exergetic and economic objectives, respectively and F is the combined objective. In this project a genetic algorithm (GA) has been selected for optimization of the problem. The assumptions that are represented in Table 6 are considered for applying GA. Decision variables are recognized by sensitivity analysis of the system (section 3.2) and their assumed range are summarized in Table 7.

The GA results are given in Table 8 for maximization of COPs and minimization of $c_{P,tot}$ individually as well as the optimization of the combined objective function. The values of decision variables for various cases are summarized in Table 9. For each case the optimum value of decision variables are defined in Table 10.

According to the optimization results, the single objective optimization of COP_{th} results in 1.03 and 1.11% increase in COP_{th} and COP_{exe} respectively. Also the amount of c_{Ptot} decreases 7.37% in this case. The single objective optimization of COP_{exe} has exactly same results. On the other hand, the single objective optimization of c_{Ptot} causes 11.45% decline in c_{Ptot} while COP_{th} and COP_{exe} decrease 2.06 and 2.27%, respectively. The multiobjective optimization results in 1.87% and 2.03% decrease in COP_{th} and COP_{exe} while the amount of c_{Ptot} decreases 10.99%. In last case although the reduction of COPs is not too much, c_{Ptot} decreases considerably which means all objectives are partly satisfied.

Table 9: The values of decision variables for various cases

Decision variable	Base case	Single objective optimized Maximum COP_{th}	Single objective optimized Maximum COP_{exe}	Single objective optimized Minimum c_{Ptot}	Multiobjective optimized
T_{gen} (°C)	85	85	85	95	94.09
T_{eva} (°C)	10	12	12	12	11.78
P_{gen} (kPa)	1800	1850	1850	1850	1850
x_c	0.9996	0.9998	0.9998	0.9998	0.9998

Table 10: The office building characteristics

Parameter name	Value	Parameter name	Value
A_f (m^2)	0.98	Uf (W m^{-2} K^{-1})	1.04
A_g (m^2)	1.86	Ug (W m^{-2} K^{-1})	0.42
$SHGC_f$	0.063	Sa	0.9
$SHGC_{gB}$	0.23-0.65	hout (W m^{-2} K^{-1})	22.71
$SHGC_{gD}$	0.57	$\tilde{o}_{out}$ (m^3 kg^{-1})	0.88

CONCLUSION

In this article hourly Modeling of the ejector-absorption refrigeration system for cooling of an office building under various solar radiations on 21st of Jun is carried out. The performance of the system is examined by varying key parameters and single and multiobjective optimizations are carried out. The following remarks can be concluded from the obtained results:

- The exergy destruction rate of the collector is the most among all components and its y_D^* is 83%. Also 48% of the whole system investment and O&M costs rate is allocated to the collector. On the other hand the exergy destruction and loss cost rates plus investment cost rate for heat storage tank and evaporator set is more than other components.
- Hourly analysis shows that from 9 AM to 5 PM cooling load and the generator heat transfer rate increase about 40 and 67% while the auxiliary heat transfer rate decreases about 83%. More over COP_{th} and COP_{exe} increase 150 and 300% while c_{Ptot} decreases 90%. The hourly variation of exergy destruction rate and product cost per exergy unit of collector are proportional to solar insolation changes.
- The single objective optimization for maximizing COPs results in about 1.1% increase in COPs and 7.4% decrease in c_{Ptot}. The single objective optimization for c_{Ptot} minimizing lead to about 2.2 and 11.5% decline in COPs and c_{Ptot} respectively. Moreover, Multi objective optimization to maximize COPs and minimize c_{Ptot} decreases c_{Ptot} by 10.9% and COPs by about 1.9%.

Appendix A.1: To calculate the capital investment cost of a component at a specific size or capacity, following relations are used for a heat exchanger and a pump respectively [14]. (R is the representative of reference component.)

$$TCI_{hex} = TCI_{R,hex}\left(\frac{A_{hex}}{A_R}\right)^{0.6} \quad (46)$$

$$A_{hex} = \frac{\dot{Q}_{hex}}{U_{hex} \times LMTD_{hex}} \quad (47)$$

$$TCI_{pmp} = TCI_{R,pmp}\left(\frac{\dot{W}_{pmp}}{\dot{W}_R}\right)^{0.26}\left(\frac{1-\eta_{pmp}}{\eta_{pmp}}\right)^{0.5} \quad (48)$$

For the evaporator, absorber, solution heat exchanger, rectifier and condenser which are considered as heat exchanger the reference costs are available at references [14, 32] and the overall heat transfer coefficient (U_{hex}) is extracted from literature [26, 33].

The capital investment costs of the ejector, flash tank, mix chamber and expansion valves are neglected due to their small amount in compare to others [26, 34]. The capital investment costs of the components of the collector and temperature stabilizer subsystems are extracted form Apricus Company [21]. The capital investment cost should be multiplied by capital recovery factor (CRF) to convert to the annual investment cost [17].

$$Z^{CI} = \mathrm{CRF} \times \mathrm{TCI}, \mathrm{CRF} = \frac{i(1+i)^N}{(1+i)^N - 1} \quad (49)$$

In the above equation i is the interest rate and N is the lifetime of the system in years, which are considered 0.15 and 20 years respectively in this work. Annual operating and maintenance (O&M) cost consists of the cost related to capital investment and the cost related to product exergy rate [17].

$$Z^{OM} = \gamma_2(TCI) + \gamma_1 t_a \dot{X}_P + \gamma_0 \quad (50)$$

γ_0 includes all other O&M costs that are independent from the capital investment cost and product exergy rate. In this study the contribution of the capital investment cost is considered more than others. As a result γ_2 is assumed to be 1.25% and other terms are neglected [12, 22, 32]. The price of electricity used by pumps and the price of natural gas used by auxiliary heat resource is considered 0.043 \$/kWh and 0.040 \$/m^3 respectively due to prices offered by Iran energy companies.

All cost data used in an economic analysis at different years (Cd_O) must be brought to the base year (Cd_B) through cost indexes as below [17]:

$$Cd_B = Cd_O \times \frac{CIndex_B}{CIndex_O} \quad (51)$$

$Cindex_B$ and CIndex are cost indexes of the base year (in this study 2013) and original year which are extracted from Chemical engineering plant Cost Index [35].

Appendix A.2: For calculating the cooling load of the assumed office building with 81 m^2 floor area, 3.6 m ceiling height and 4 south face window (each window area is 1.2× 1.5 m^2) the following parameters are needed [29]:

REFERENCES

1. Kalogirou, S.A., 2009. Solar Energy Engineering: Processes and Systems, Elsevier Science.
2. Alvares, S.G. and C. Trepp, 1987. Simulation of a solar driven aqua-ammonia absorption refrigeration system Part 1: mathematical description and system optimization, International Journal of Refrigeration, 10: 40-48.
3. Atmaca, I. and A. Yigit, 2003. Simulation of solar-powered absorption cooling system, Renewable Energy, 28: 1277-1293.
4. Ozgoren, M., M. Bilgili and O. Babayigit, 2012. Hourly performance prediction of ammonia-water solar absorption refrigeration, Applied Thermal Engineering, 40: 80-90.
5. Hamed, M., A. Fellah and A. Ben Brahim, 2012. Optimization of a solar driven absorption refrigerator in the transient regime, Applied Energy, 92: 714-724.
6. Sun, D., I.W. Eames and S. Aphornratana, 1996. Evaluation of a novel combined ejector-absorption refrigeration cycle - I: computer simulation, International Journal of Refrigeration, 19: 172-180.
7. Aphornratana, S. and I.W. Eames, 1998. Experimental investigation of a combined ejector-absorption refrigerator, Int. J. Energy Res. 22(3): 195-207.
8. Hong, D., G. Chen, L. Tang and Y. He, 2011. A novel ejector-absorption combined refrigeration cycle, International Journal of Refrigeration, 34: 1596-1603.
9. Sözen, A. and M. Özalp, 2005. Solar-driven ejector-absorption cooling system, Applied Energy, 80: 97-113.
10. Sirwan, R., M.A. Alghoul, K. Sopian and Y. Ali, 2013. Thermodynamic analysis of an ejector-flash tank-absorption cooling system, Applied Thermal Engineering, 58: 85-97.
11. Sirwan, R., M.A. Alghoul, K. Sopian, Y. Ali and J. Abdulateef, 2013. Evaluation of adding flash tank to solar combined ejector-absorption refrigeration system, Solar Energy, 91: 283-296.
12. Misra, R.D., P.K. Sahoo, S. Sahoo and A. Gupta, 2003. Thermoeconomic optimization of a single effect water/LiBr vapour absorption refrigeration system, International Journal of Refrigeration, 26: 158-169.
13. Rubio-Maya, C., J.J. Pacheco-Ibarra, J.M. Belman-Flores, S.R. Galván-González and C. Mendoza-Covarrubias, 2012. NLP model of a LiBr-H2O absorption refrigeration system for the minimization of the annual operating cost, Applied Thermal Engineering, 37: 10-18.
14. Garousi Farshi, L., S.M.S. Mahmoudi and M.A. Rosen, 2013. Exergoeconomic comparison of double effect and combined ejector-double effect absorption refrigeration systems, Applied Energy, 103: 700-711.
15. Klein, S. and F. Alvarado, Engineering equation solver, Http://Www.Fchart.Com.
16. Hengel, Y.A. and M.A. Boles, 2006. Thermodynamics: an engineering approach, McGraw-Hill Higher Education.
17. Bejan, A., G. Tsatsaronis and M.J. Moran, 1996. Thermal Design and Optimization, Wiley.
18. He, L.J., L.M. Tang and G.M. Chen, 2009. Performance prediction of refrigerant-DMF solutions in a single-stage solar-powered absorption refrigeration system at low generating temperatures, Solar Energy, 83: 2029-2038.
19. Wang, M., J. Wang, Y. Zhao, P. Zhao and Y. Dai, 2013. Thermodynamic analysis and optimization of a solar-driven regenerative organic Rankine cycle (ORC) based on flat-plate solar collectors, Applied Thermal Engineering, 50: 816-825.
20. Pongtornkulpanich, A., S. Thepa, M. Amornkitbamrung and C. Butcher, 2008. Experience with fully operational solar-driven 10-ton LiBr/H2O single-effect absorption cooling system in Thailand, Renewable Energy, 33: 943-949.

21. Http://Www.Apricus.Com.Au product specification sheet, 2013.
22. Misra, R.D., P.K. Sahoo and A. Gupta, 2006. Thermoeconomic evaluation and optimization of an aqua-ammonia vapour-absorption refrigeration system, International Journal of Refrigeration, 29: 47-59.
23. Kotas, T.J., 1995. The Exergy Method of Thermal Plant Analysis, Krieger Publishing Company.
24. Frangopoulos, C.A. and U. Staff, Exergy, Energy System Analysis and Optimization, 2009. EOLSS Publishers Company Limited.
25. Al-Sulaiman, F.A., I. Dincer and F. Hamdullahpur, 2011. Exergy modeling of a new solar driven trigeneration system, Solar Energy, 85: 2228-2243.
26. Zare, V., S.M.S. Mahmoudi, M. Yari, 2013. An exergoeconomic investigation of waste heat recovery from the Gas Turbine-Modular Helium Reactor (GT-MHR) employing an ammonia-water power/cooling cycle, Energy, 61: 397-409.
27. Kreith, F., 2000. CRC Handbook of Thermal Engineering, Taylor & Francis.
28. https://eosweb.larc.nasa.gov, 2013.
29. McQuiston, F.C., J.D. Parker and J.D. Spitler, 2005. Heating, ventilating and air conditioning: analysis and design, John Wiley & Sons.
30. Abdulateef, J., M. Alghoul, A. Zaharim and K. Sopian, 2009. Experimental Investigation on Solar Absorption Refrigeration System in Malaysia, in: Proceedings of the 3rd Wseas Int. Conf. On Renewable Energy Sources, pp: 1-3.
31. Sayyaadi, H., A. Saffari and A. Mahmoodian, 2010. Various approaches in optimization of multi effects distillation desalination systems using a hybrid meta-heuristic optimization tool, Desalination, 254: 138-148.
32. Zare, V., S.M.S. Mahmoudi, M. Yari and M. Amidpour, 2012. Thermoeconomic analysis and optimization of an ammonia-water power/cooling cogeneration cycle, Energy, 47: 271-283.
33. Gebreslassie, B.H., G. Guillén-Gosálbez, L. Jiménez and D. Boer, 2012. Solar assisted absorption cooling cycles for reduction of global warming: A multi-objective optimization approach, Solar Energy, 86: 2083-2094.
34. Gebreslassie, B.H., G. Guillén-Gosálbez, L. Jiménez and D. Boer, 2009. Design of environmentally conscious absorption cooling systems via multi-objective optimization and life cycle assessment, Applied Energy, 86: 1712-1722.
35. Economic Indicators, Chemical engineering plant Cost Index (CEPCI), Chemical engineering, (September 2013).

Persian Abstract

چکیده

این مقاله یک سیستم تبرید جذبی-اجکتوری بهبودیافته را به منظور تأمین بار سرمایش یک ساختمان اداری پیشنهاد و مورد بررسی قرار می دهد. مدلسازی ساعتی عملکرد سیستم بر اساس مدلسازی بار سرمایش مورد نیاز ساعتی و نرخ شدت تابش ساعتی خورشید در روز ۲۱ ام جولای با حداکثر تابش خورشیدی انجام شده است. نتایج نشان می دهد که ضریب عملکرد ترمودینامیکی (COPth) و ضریب عملکرد اگزرژتیک (COPexe) به ترتیب ۱۵۰ و ۳۰۰٪ افزایش می یابد. در حالیکه قیمت تولید واحد اگزرژی کل سیستم (cPtot) به اندازه ۹۰٪ کاهش می یابد. نتایج تحلیل ترمودینامیکی و ترمواکونومیکی اثر پارامترهای مؤثر بر COPth، COPexe وcPtot را تخمین می زند. همچنین بهینه سازی تک هدفه و چندهدفه برای حداکثر COPها و حداقل کردن cPtot صورت گرفته است. بر اساس بهینه سازی تک هدفه جهت حداکثر کردن ضرایب عملکرد و کاهش قیمت تولید واحد اگزرژی کل سیستم، COPها ۱/۱٪ افزایش و cPtot به میزان ۷/۴٪ کاهش می یابد. همچنین بهینه سازی تک هدفه برای مینیمم کردن cPtot منجر به کاهش ۲/۲٪ ضرایب عملکرد و کاهش ۱۱/۵٪ قیمت تولید واحد اگزرژی کل سیستم می شود. در آخر بهینه سازی چندهدفه برای حداکثر کردن ضرایب عملکرد ترمودینامیکی و اگزرژتیک و حداقل کردن cPtot بطور همزمان، منجر به کاهش ۱/۹ ٪ ضرایب عملکرد و کاهش ۱۰/۹٪ قیمت تولید واحد اگزرژی کل سیستم می شود.